Atmospheric Environment 317 (2024) 120199

Contents lists available at ScienceDirect

Atmospheric Environment

journal homepage: www.elsevier.com/locate/atmosenv

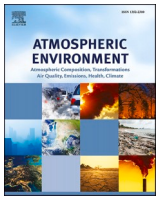

Declines of gaseous element mercury concentrations at an urban site in eastern China caused by reductions of anthropogenic emission

Peng Sun [a], Zhengcheng Song [b,*], Yanhong Qin [a], Zheng Xu [a], Yanxu Zhang [b], Sheng Zhong [a], Jianqiao Yu [a]

[a] Jiangsu Environmental Monitoring Center, Nanjing, China
[b] Joint International Research Laboratory of Atmospheric and Earth System Research, School of Atmospheric Sciences, Nanjing University, Nanjing, China

HIGHLIGHTS

- Long-term decreasing trend of GEM was observed at an urban site in eastern China.
- The decrease in anthropogenic emissions was mostly responsible for the GEM decreases.
- The joint efforts to reduce air pollution also had a major impact on GEM's decrease.

ARTICLE INFO

Keywords:
Atmospheric Hg
Long-term trends
Anthropogenic emissions
Source apportionment
GEOS-Chem model

ABSTRACT

Long-term observations (June 2014 to June 2022) of atmospheric mercury (Hg) mass concentrations were conducted at an urban site in Nanjing, eastern China, together with other air pollutants. Throughout the sampling period, gaseous elemental mercury (GEM) exhibited a substantial decline from 5.41 ± 1.49 ng m^{-3} in 2014 to 2.17 ± 1.26 ng m^{-3} in 2022. The monthly mean concentrations of GEM displayed a significant downward trend, with a rate of 0.36 ng m^{-3} yr^{-1} (−7% yr^{-1}). To identify the potential sources contributing to the observed GEM levels, positive matrix factorization (PMF) analysis was employed in conjunction with other relevant pollutants. The results revealed that the natural and anthropogenic emissions played comparable roles in shaping the measured GEM concentrations, with the reduction of coal combustion emissions being the primary driver behind the observed declines at this site. Furthermore, GEOS-Chem simulations suggested a substantial reduction of anthropogenic emissions in eastern China in recent years. This study highlights the decreasing trend of GEM concentrations in eastern China over the past decade, which is attributed to the combined efforts in air pollutant controls, resulting in the synergistic mitigation of Hg from the atmosphere.

1. Introduction

Mercury (Hg) is a highly toxic neurotoxin that poses significant health risks to both humans and wildlife (Wu et al., 2020; Zhang et al., 2021). Once released into the atmosphere, mercury can be transported globally through atmospheric circulation, leading to widespread Hg pollution (Holmes et al., 2010; Selin et al., 2008). Atmospheric Hg originates from both natural sources, such as volcanic eruptions, hydrothermal vents, and anthropogenic activities, including coal combustion and industrial processes (Beckers and Rinklebe, 2017; Obrist et al., 2018). Since the Industrial Revolution, anthropogenic emissions have caused global atmospheric Hg deposition fluxes to increase approximately three to four times compared to pre-industrial levels (Obrist et al., 2018; UN-Environment, 2019). Recent research indicates that the global health effects of methylmercury (MeHg) exposure for the general population amount to $117 per year at present levels (Zhang et al., 2021). In order to mitigate the detrimental effects of Hg exposure on human health, the *Minamata Convention on Mercury* was implemented worldwide in August 2017 (UNEP, 2013).

Atmospheric Hg is mainly in the form of gaseous elemental Hg (Hg^0, GEM) (>90%) that can retain in the air for months, enabling its global transport (Shah et al., 2021; Zhang et al., 2023b). GEM can undergo oxidation by oxidants such as bromine (Br), chlorine (Cl), hydroxyl radicals (OH), and ozone (O_3), leading to the formation of gaseous

* Corresponding author.
E-mail address: songzc@nju.edu.cn (Z. Song).

https://doi.org/10.1016/j.atmosenv.2023.120199
Received 10 August 2023; Received in revised form 26 October 2023; Accepted 6 November 2023
Available online 13 November 2023

oxidized mercury (Hg^{2+}, GOM), which can be absorbed onto particulate matter, forming particle-bound mercury (HgP, PBM) (Horowitz et al., 2017; Shah et al., 2021). Both GOM and PBM are water-soluble and can be efficiently removed from the atmosphere through wet and dry deposition processes (Pacyna et al., 2016; Saiz-Lopez et al., 2018). Consequently, the residence time of GOM and PBM in the atmosphere is shorter than that of GEM, typically ranging from several days to weeks. Deposited Hg can be partially re-emitted into the air from land and ocean surfaces, contributing to the complexity of the global biogeochemical Hg cycle.

China has emerged as the world's largest emitter of Hg in recent decades. In 2010, China's reported atmospheric Hg emissions amounted to 538 tons, with coal combustion, non-ferrous metal smelting, and cement production sectors identified as the main sources (Zhang et al., 2015a). The intense anthropogenic Hg emissions have resulted in significantly higher atmospheric Hg levels in China compared to developed countries. For instance, average GEM concentrations at remote sites in China are much higher than the background levels in the Northern Hemisphere (Fu et al., 2015; Zhang et al., 2016). And atmospheric Hg wet deposition in China is substantially elevated (by a factor of 2.6–3.6) compared to North America and Europe (Fu et al., 2016). Since 2013, China has implemented aggressive measures to control air pollution, resulting in simultaneous reductions in anthropogenic Hg emissions (Liu et al., 2019; Wu et al., 2016). Consequently, atmospheric Hg pollution in China has shown signs of improvement. Wu et al. (2023) observed rapid declines (−4% to −2% yr^{-1}) in GEM levels at two mountain sites over the past 5–7 years. Tang et al. (2018) reported a decrease in GEM levels from 2.68 ± 1.07 ng m^{-3} to 1.60 ± 0.56 ng m^{-3} between 2014 and 2016 at Chongming Island. Qin et al. (2020) documented a significant decrease in GEM levels from 3.01 ng m^{-3} in 2015 to 2.03 ng m^{-3} in 2018 in Shanghai. However, existing studies on atmospheric Hg trends in urban areas only cover short periods of 3–4 years. To provide an accurate assessment of the perceived improvement in atmospheric Hg resulting from emission reductions, continuous long-term observations in urban areas are still lacking.

In this study, we present the long-term (2014–2022) observed reduction of atmospheric Hg levels and other air pollutants (e.g., SO_2, $PM_{2.5}$, NO_2, etc.) at an urban site in Nanjing, eastern China. The annual and seasonal variations of GEM were comprehensively analyzed to investigate the factors influencing these variations. Moreover, we develop different methods, including positive matrix factorization (PMF) and a global atmospheric model (GEOS-Chem) to quantify the contributions of different sources to the observed decline of atmospheric Hg at the observation site. The model provides estimation of the possible reduction rates of anthropogenic emissions in eastern China in recent years, and the discrepancies between the observations and model results were further discussed.

2. Method

2.1. Site descriptions

The sampling site is located at Jiangsu Environment Monitoring Center in Nanjing, a typical megacity in the Western Yangtze River delta (YRD) of eastern China (Fig. 1). It is influenced by multiple sources, including industry, traffic, cooking, and biogenic emissions, thus representative of an urban site. More detailed descriptions of this sampling site can be found in previous studies (Zhang et al., 2015b).

2.2. Sampling methods and analysis

Atmospheric Hg concentrations including GEM, GOM, and PBM were continuously measured by using the Tekran 2537 analyzer (Tekran Inc., Model 1130A, Canada) with a sensitivity of <0.1 ng m^{-3} from June 2014 to June 2022 at several-hour resolution. GEM was measured at the sampling frequency of 5 min, GOM and PBM were in the frequency of 1 h

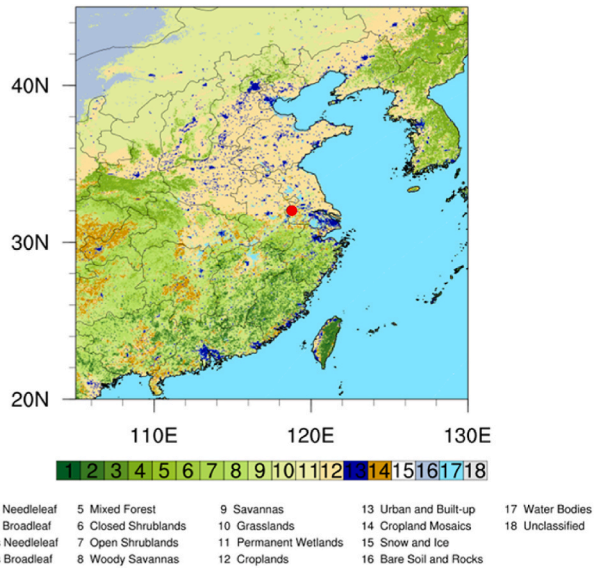

Fig. 1. The specific position of Jiangsu Environment Monitoring Center in Nanjing together with the types of land cover (https://lpdaac.usgs.gov/dataset_discovery/modis/modis_products_table/mcd12q1_v006).

with the carrier gas flow rate of 10 L min^{-1}. By using the gold preconcentration with atomic fluorescence detection, atmospheric Hg was trapped in the units and then thermally decomposed as the form of GEM, and finally, GEM was detected by the high-sensitivity CVAFS detector. During the long-term sampling period, we conducted regular and reasonable maintenance on the analyzer, including the replacement of the drying tubes and quartz filters following the methods in Tekran technical notes. The analyzer was automatically calibrated using its internal permeation source at a frequency of 47 h. It should be noted that the discontinuities of the data at the beginning of the study were due to the instrument maintenance and other field observations elsewhere.

The instruments also included a MARGA (ten Brink et al., 2007) to measure gas NH_3 and NH_4^+ in aerosols, and an EHM-X200 (Skyray Instrument: www.skyray-instrument.com) based on X-ray fluorescence to measure trace elements (Fe, Mn, V) in $PM_{2.5}$. Trace gases (i.e., SO_2, NO_x, CO) and $PM_{2.5}$ mass concentrations were also measured at the site, together with meteorological data including temperature and relative humidity (Zhang et al., 2015b).

2.3. Source apportionment

Positive matrix factorization. The positive matrix factorization (PMF) analysis, utilizing the PMF2. exe algorithm introduced by Paatero and Tapper (1994), was conducted on the combined dataset to quantify the contributions of Hg emissions from natural surfaces and anthropogenic sources to ambient GEM concentrations. To achieve this, specific variables related to natural surface emissions or anthropogenic sources were introduced as tracers, as described by Qin et al. (2020). Only species exhibiting distinct characteristics were included in the analysis matrix. A dataset incorporating uncertainty values for each species was generated and incorporated into the model, assuming an error fraction of 15% for GEM concentrations and 10% for other compounds, following Qin et al. (2020). Considering that gas NH_3 emissions from the soil are temperature-dependent, NH_3 has been recognized as a tracer for natural sources (Qin et al., 2020). However, some studies also demonstrated that the gas NH_3 concentrations were substantially affected by the thermodynamic equilibrium of ammonium nitrate (Sun et al., 2018), we thus considered total ammonia (gas NH_3 aerosol NH_4^+) in the matrix to be one tracer of natural sources. The PMF analysis was performed using an Igor Pro-based PMF Evaluation Tool with the daily time resolution data and the results were evaluated following the procedures

outlined in Ulbrich et al. (2009). The specific procedures for GEM sources apportionment are described in detail in Text S1. Based on the factor profiles, the temporal variations, and the Q/Qexp metric, a 4-factor solution with fpeak = 0 was chosen as the optimum solution. This solution resolved a natural source factor, a coal-combustion factor, a vehicle-emission factor, and an industrial factor.

GEOS-Chem model. In this study, we employed the GEOS-Chem (Goddard Earth Observing System-Chemistry) model (www.geos-chem.org; version 12.9.0) as described by Shah et al. (2021). The model utilizes assimilated meteorological data from the Goddard Earth Observation System (GEOS) general circulation model, provided by the NASA Global Modeling and Assimilation Office (GMAO), at a resolution of 4° (latitude) × 5° (longitude). Hg emissions from Horowitz et al. (2017) were incorporated into the model, along with gridded land and ocean surface Hg concentrations as boundary conditions. The mercury inventory encompasses natural emissions from geogenic, biomass, soil, snow, and ocean sources. The model accounts for the re-emission process of atmospheric deposited Hg, where 20% of the deposited Hg can be re-emitted into the air from land surfaces. The model tracks three Hg species: Hg^0, Hg^{2+}, and HgP. The conversion between Hg^{2+} in the gas phase and the aerosol/cloud phase is treated as a kinetic process, following the approach of Amos et al. (2012). Notably, the model incorporates the latest advancements in atmospheric Hg chemistry, including comparable oxidation of global Hg^0 to Hg^{II} by Br and OH radicals (Shah et al., 2021). We simulate five years with different anthropogenic emissions from 2017 to 2021, while keeping natural emissions consistent throughout the simulations. We conducted a 3-y simulation for each year, and the initial two years were used for model initialization, and the third year was employed for result analysis.

Anthropogenic emission inventory. The GEOS-Chem simulation need Hg emissions from global anthropogenic sectors. However, comprehensive studies on global anthropogenic Hg emissions in recent years are still lacking. In this study, we developed an emission inventory spanning from 2017 to 2021. Previous research by Liu et al. (2019) revealed a 22% reduction in total Hg emissions in China from 2013 to 2017, corresponding to a reduction rate of 5% yr^{-1}. More recent research by Zhang et al. (2023a) established anthropogenic Hg emissions in China from 2010 to 2020, showing a comparable average reduction rate of 3.4% yr^{-1}. Taking this information into account, we utilized an annual reduction rate of 5% for China's emission in our study. Using the global emissions data from Streets et al. (2019) as a baseline, we scaled China's Hg emissions to construct an inventory of global atmospheric Hg emissions from 2017 to 2021. Hg emissions in other countries remained consistent during this period.

3. Results and discussions

3.1. Observed atmospheric Hg and air pollutants trends

The annual average GEM concentrations in urban Nanjing exhibited a decline from 5.41 ± 1.49 ng m^{-3} in 2014 to 2.17 ± 1.26 ng m^{-3} in 2022, with a rate of 0.36 ± 0.03 ng m^{-3} yr^{-1} (−7±0.6% yr^{-1}). The observed PBM and GOM also depict significant declines with the rates of −7% yr^{-1} and -13% yr^{-1} as shown in Fig. S2. This decreasing trend mirrors the concurrent trends observed in other air pollutants at the same site (Fig. 2). Over the observation period, $PM_{2.5}$, SO_2, NO_2, CO, and total NH_3 demonstrated decreasing rates of −7±0.9% yr^{-1}, -10 ± 0.6% yr^{-1}, -5±0.9% yr^{-1}, -4±0.8% yr^{-1}, and -3±0.6% yr^{-1}, respectively (Fig. 2). Notably, SO_2 exhibited the highest reduction rate. These findings indicate the remarkable success achieved in air pollution control in the Yangtze River Delta region, which is a major industrial base characterized by significant coal consumption. The success can be attributed to desulfurization equipment implemented in power plants and factories, as well as the transition from coal to natural gas and electricity in recent years (Ding et al., 2019).

Research has shown that aggressive control measures for air pollutants can also lead to a simultaneous reduction in anthropogenic Hg emissions, as Hg is synergistically removed from tail gas (Liu et al., 2019; Wu et al., 2018). The correlation coefficients between GEM and other air pollutants are presented in Table S1. Notably, GEM exhibits a

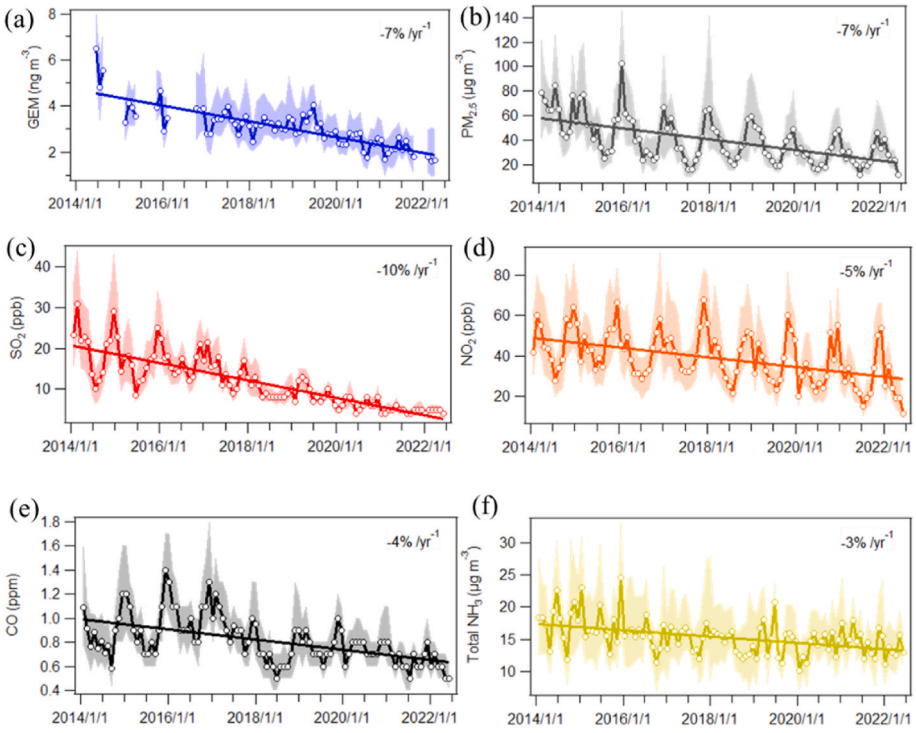

Fig. 2. Monthly statistics and trends for (a) GEM, (b) $PM_{2.5}$, (c) SO_2, (d) NO_2 (e) CO, and (f) total NH_3 observed in this study. The solid lines marked with open circles represent the monthly medium value, and shaded areas mark the data from the 25th to 75th percentiles. Solid lines show the linear regression fitting for measurement data.

strong correlation with SO_2 ($R^2 = 0.37$, $P < 0.05$), suggesting potential common sources. However, the lower rate of decline in GEM compared to SO_2 indicates the presence of other sources, such as natural emissions, contributing to the total GEM levels. In addition, the observed long-term declines in air pollutants (Fig. 2) may impact the atmospheric Hg species and their deposition on land, subsequently influencing the re-emission of GEM from land surfaces. The strong correlation ($R^2 = 0.33$, $P < 0.05$) between monthly PBM and $PM_{2.5}$ indicates the absorption of gaseous Hg by fine particles.

Fig. 3 illustrates the significant seasonality of atmospheric Hg and air pollutant concentrations. GOM shows peak levels in summer, while PBM peaks in winter, and GEM exhibits peaks in both summer and winter seasons. The seasonal variation of GEM demonstrates a significant positive correlation with total NH_3 ($R^2 = 0.56$, $P < 0.05$) as both are influenced by natural and anthropogenic sources (Qin et al., 2020). The observed winter peaks in atmospheric Hg align with findings from other studies conducted in mainland China, which are attributed to emissions from fossil fuel combustion for heating purposes (Fu et al., 2015; Liu et al., 2019). The seasonal concentrations of PBM display a positive correlation with $PM_{2.5}$ ($R^2 = 0.86$, $P < 0.05$), indicating the absorption of gaseous Hg by fine particles. Additionally, the positive correlation between the seasonal variation of O_3 and GOM ($R^2 = 0.6$, $P < 0.05$) suggests that the oxidation of Hg^0 by O_3 in the ambient air contributes to the observed patterns. The positive correlations of seasonal GOM and PBM with native air pollutants imply their dependence on local chemical processes. The year variations of GEM and other pollutants during four seasons are discussed in Text S2.

To investigate further insights into the declining trends of atmospheric GEM, we compiled available data on GEM trends in China's urban areas in Table 1. Our study stands out as it covers the longest observation period, spanning from 2014 to 2022, whereas other studies provide GEM data for only 3–4 years. Consistent with our findings in Nanjing, reductions in GEM concentrations have also been observed in Shanghai (−0.32 to −0.60 ng m^{-3} yr^{-1}) and Beijing (−0.37 ng m^{-3} yr^{-1}). These decline rates are comparable to the observation in Nanjing (−0.36 ng m^{-3} yr^{-1}). Notably, when compared with global declines in GEM, our observed reduction rates (−7% yr^{-1}) surpass those observed in Europe and North America (−1% to −2% yr^{-1}) between 1990 and 2013 (Zhang et al., 2016). This stark contrast indicates the significant progress made by China in effectively mitigating atmospheric Hg pollution through comprehensive air pollution control measures. Furthermore, when we combine our analysis with two Shanghai-based studies (Tang et al., 2018; Qin et al., 2020), we see that GEM concentrations in eastern China have been declining for the previous ten years.

Table 1
Observations of GEM concentrations trends in urban areas of China.

No.	Observation site	Years	Decline rates (ng m^{-3} yr^{-1})	Range of GEM (ng m^{-3})	Reference
1	Nanjing	2014–2022	0.36	2.17–5.41	This study
2	Shanghai	2014–2016	0.60 ± 0.08	1.60–2.68	Tang et al., 2018
3	Shanghai	2015–2018	0.32 ± 0.07	2.03–3.01	Qin et al. (2020)
4	Beijing	2015–2018	0.37	2.72–4.61	Wu et al. (2020)

3.2. Source apportionment of observed GEM

The relationships between atmospheric GEM and other pollutants can provide valuable insights into the sources of GEM. As illustrated in Fig. 4, there is a positive correlation between monthly variations of GEM and $PM_{2.5}$ ($R^2 = 0.21$, $P < 0.05$) as well as SO_2 ($R^2 = 0.36$, $P < 0.05$), suggesting their shared origins. Points above the fitted line, particularly during periods of high temperature, indicate the influence of temperature on atmospheric GEM levels, potentially suggesting contributions from natural emissions because GEM re-emission from land is temperature sensitive (Zhu et al., 2016). While little influence of RH on GEM was found (Fig. S4).

To further elucidate the emission sources and quantify their contributions to GEM mass concentrations in Nanjing, we employed the PMF model on combined matrix data. The model was conducted exclusively on the dataset spanning from 2017 to 2021, encompassing a full year time. Based on the optimal results of the PMF analysis (Text S1, Fig. 5), four source factors contributing to GEM were identified. In Fig. S5, the factor exhibiting the highest loadings of SO_2 was attributed to coal

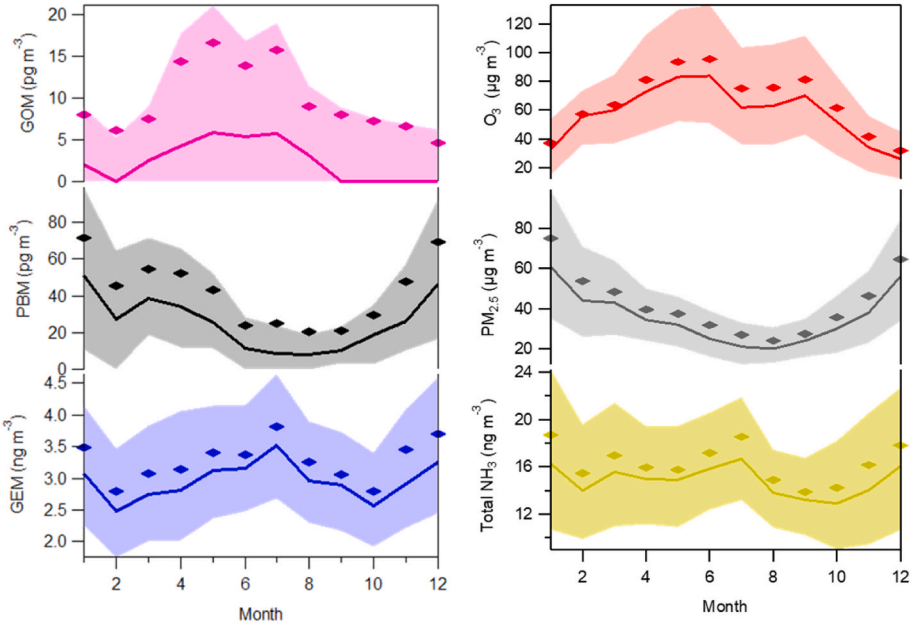

Fig. 3. Seasonality of atmospheric Hg and air pollutants. (a) Reactive gaseous mercury (GOM). (b) Particle-bound mercury (PBM). (c) Gaseous element mercury (GEM). (d) Ozone (O_3). (e) Fine particulate matter ($PM_{2.5}$). (f) Total NH_3 (gas NH_3 and particulate NH_4^+). Bold solid lines are the median values; shaded areas represent percentiles of 75% and 25% and diamonds represent the mean values.

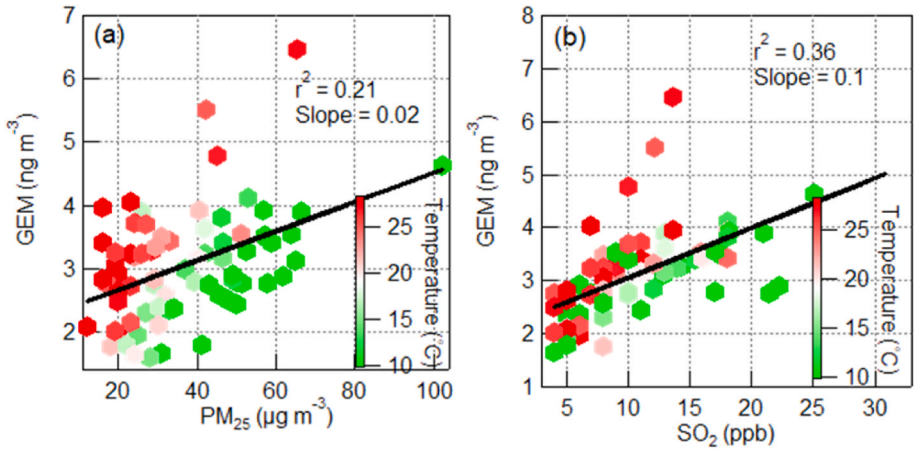

Fig. 4. The scatter plots that compare the GEM concentrations versus (a) $PM_{2.5}$ mass concentrations; (b) SO_2 mass concentrations. The map is color-coded with air temperature.

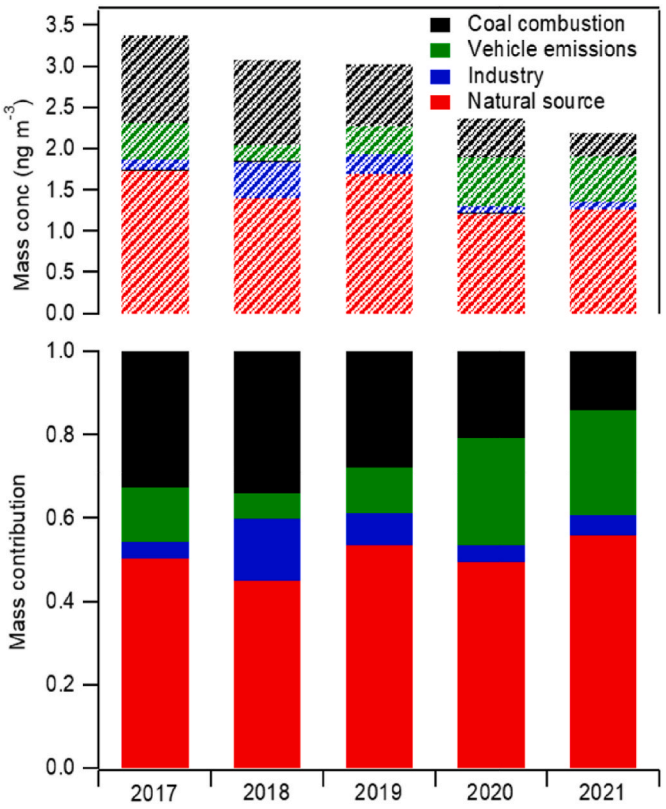

Fig. 5. Mass concentrations and contributions of different sources interpreted by PMF model from 2017 to 2021.

combustion, accounting for 26% of GEM. The vehicle emission factor is characterized by relatively high loadings of NO_2 (Wang et al., 2021), contributing 16% to GEM. Another industrial emission factor (excluding combustion processes) played a substantial role in V, Fe, and Mn emissions, which are considered typical tracers of industrial production (Qin et al., 2020), with a contribution of 7%. The remaining factor accounted for 51% of the total contribution and was influenced by temperature, suggesting a natural source due to its high temperature dependency (Zhu et al., 2016). Overall, the PMF analysis allocated comparable contributions of 49% for anthropogenic emissions and 51% for natural emissions to the GEM levels. These findings align with previous studies indicating that surface land emissions of Hg in China are comparable to those from anthropogenic activities (Wang et al., 2016, 2018). Importantly, the primary natural emissions at this site is speculated to be the previously cumulated Hg on land due to two reasons: i) high levels of Hg emissions and atmospheric deposition, urban areas in China typically experience significant Hg pollution, including soil contamination, creating conditions conducive to Hg release from land (Li et al., 2017; Liu et al., 2021; Song et al., 2021); ii) the positive correlation observed between GEM concentrations and temperature, as well as total NH_3, as discussed earlier, further supports the notion of Hg released from land sources.

The factor associated with coal combustion has exhibited a significant decline, dropping from 1.1 ng m^{-3} in 2017 to 0.3 ng m^{-3} in 2021 (Fig. 5). This factor contributed to 44%–61% of the observed GEM declines, corresponding to a decrease of −6% to −4% yr^{-1} considering the overall GEM decline rate of −9% yr^{-1} during this period. The contributions from the vehicle and other industrial emissions to the GEM decline were minimal, with mass concentrations fluctuating within 0.5 ng m^{-3}. Mass concentrations from natural emission sources also experienced a decline, decreasing from 1.7 ng m^{-3} in 2017 to 1.1 ng m^{-3} in 2021. The nature source contributed to 37%–53% of the declines and caused a GEM decrease of approximately −5% to −3% yr^{-1}. According to the PMF results, the reduction in coal combustion and natural sources accounted for the majority of the GEM declines. The analysis below provides comprehensive explanations.

Since 2013, China has implemented a series of crucial air pollution control measures to reduce the emission of air pollutants (Zheng et al., 2018). These measures include the application of air pollution control devices to remove conventional pollutants such as $PM_{2.5}$, SO_2, and NO_X, which also possess the ability to co-remove Hg. A study indicates that a significant portion of Hg in coal-fired power plants can be oxidized, captured, and subsequently removed from the production processes, with removal rates reaching up to 90% (Zhao et al., 2019). Field investigations on unit emissions have demonstrated that total Hg emissions in China reduced by 22% from 2013 to 2017, with coal-fired power plants and industrial boilers accounting for 68% of the reduction (Liu et al., 2019). With the increased adoption of cleaner technologies and the more stringent local emission standards for the YRD region in recent years (Zhang et al., 2023a), our observation shows that the success of ultralow emission from coal combustion sectors in eastern China is evident in the control of atmospheric Hg concentrations. In our study site, we suppose the continuous declines of atmospheric Hg might lessen the intensity of Hg deposition, which then might decrease the accumulation of Hg on land and, as a result, reduce the GEM released from land nature sources (e.g., soil). Because the Hg re-emission from soil has the potential to affect local atmospheric Hg (Zhu et al., 2018, 2022). Taking into account the small contribution from temperature fluctuations

(Texs2, Fig. S2c), these processes are thought to be the cause of the natural-source Hg emissions at our study site reducing over the years (Fig. S3).

3.3. Reduction of anthropogenic emissions

The GEOS-Chem simulations are conducted to connect the anthropogenic reduction with the declines of GEM concentrations in eastern China. By employing our revised inventory (see section 2.3) and maintaining consistent meteorological conditions and natural emissions, the model effectively isolated the impact of anthropogenic emissions. Fig. 6 depicts a comparison between the observed and simulated annual mean concentrations of GEM in Nanjing from 2017 to 2021. The simulated GEM concentrations align with the lower end of the observed data, falling within the range of observation and model representation error. We speculate that the relatively lower GEM may be attributed to the coarse resolution of the model, which may cause underestimation for the simulation results (Xu et al., 2022; Zhang et al., 2012). The GEOS-Chem simulations successfully capture a declining trend in GEM concentrations, with a rate of −2.4% yr^{-1}. During this period, the observed decline rate of GEM was −9% yr^{-1}, with −6% to −4% yr^{-1} attributed to anthropogenic emissions resolved by PMF analysis (Fig. 6). This decline rate is approximately twice the rate of our GEOS-Chem modeled results.

The discrepancy between model and PMF analysis may stem from three factors. Firstly, the model underestimates the reduction rate in anthropogenic emission. Recent research has reported an average reduction rate of 3.4% yr^{-1} for Hg emissions in China over the past decade, with eastern and central China contributing the most to the reduction from 2015 to 2020 (Zhang et al., 2023a). This suggests that the reduction in anthropogenic emissions at our study site, would likely exceed the average level of 3.4% yr^{-1} during recent years. In our model, the utilization of an average reduction rate of 5% yr^{-1} for eastern China's emissions appears to be insufficient. Secondly, the impact of global emission reductions is ignored in our model, as we kept Hg emissions from other countries consistent. The implementation of the *Minamata Convention on Mercury* worldwide since 2017 implies the potential reduction of global anthropogenic emissions in recent years. Global reductions in Hg emissions may lead to a decline in background atmospheric Hg concentrations, which would contribute to the reductions of cumulated Hg on land and observed declines in atmospheric GEM levels in China. However, the effectiveness of the convention in reducing global anthropogenic Hg emissions and its impact on atmospheric Hg levels have yet to be evaluated. We, therefore, propose that studies in this field should be carried out urgently. Thirdly, the GEOS-Chem data should be representative of a regional average in eastern China due to its coarse resolution. Because the model average includes both rural and urban areas, it is also likely to underestimate the drop rate at our study urban site. As it is reported that the annual drop rate of GEM in rural China (−4% to −2% yr^{-1}) is lower than that of our urban location (−7% yr^{-1}) (Wu et al., 2023). Despite the potential underestimation of the simulated decline rate, our findings highlight the significant role of decreasing anthropogenic emissions in driving the decline of GEM in eastern China.

4. Conclusions

Our research reveals that the observed decrease in GEM in eastern China is primarily attributed to the reduction of anthropogenic Hg emissions. Long-term observations of GEM and other conventional pollutants, such as $PM_{2.5}$, SO_2, and NO_2, consistently show declines from 2014 to 2022 in eastern China, resulting from the aggressive air pollution control measures implemented. The PMF receptor model identifies the reduction of coal combustion emissions as the main driver of the long-term decline in GEM concentrations. Furthermore, GEOS-Chem simulations indicate a remarkable reduction of anthropogenic Hg emissions in eastern China from 2017 to 2021. This study underscores China's significant achievements in atmospheric Hg control, which have contributed significantly to the objectives of the *Minamata Convention on Mercury*.

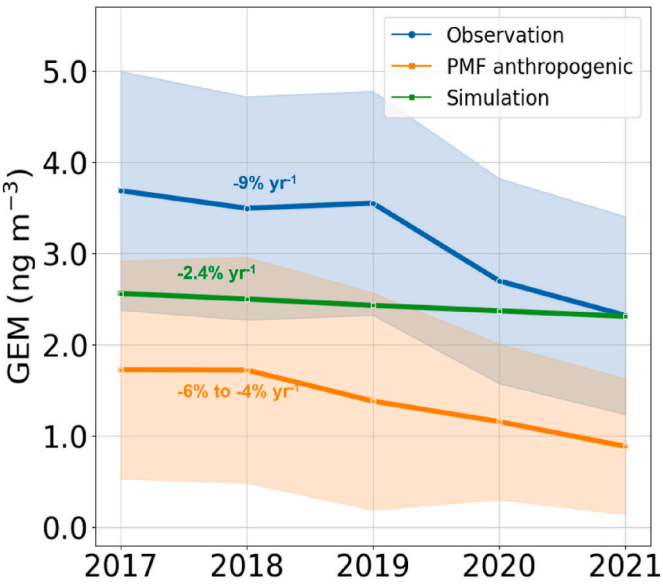

Fig. 6. Regional trends in GEM concentrations. Observations for individual years are shown as the blue line, GEOS-Chem simulations for 5% yr^{-1} reduction of anthropogenic emissions are shown as the green line, and PMF-resolved anthropogenic mass concentrations for GEM are shown as the yellow line. The shaded areas mark the standard deviations of the data.

CRediT authorship contribution statement

Peng Sun: Conceptualization, Formal analysis, Funding acquisition, Investigation, Methodology, Software, Visualization, Writing – original draft, Writing – review & editing. **Zhengcheng Song:** Conceptualization, Formal analysis, Writing – original draft, Writing – review & editing, Methodology, Software, Visualization. **Yanhong Qin:** Data curation, Resources. **Zheng Xu:** Data curation, Resources. **Yanxu Zhang:** Supervision, Writing – review & editing, Formal analysis. **Sheng Zhong:** Validation, Data curation, Conceptualization. **Jianqiao Yu:** Project administration, Resources.

Declaration of competing interest

All the authors declare that they have no known competing financial interests or personal relationships that could have appeared to influence the work reported in this paper.

Data availability

Data will be made available on request.

Acknowledgments

This study was supported by the National Natural Science Foundation of China (42105096/41975154).

Appendix A. Supplementary data

Supplementary data to this article can be found online at https://doi.org/10.1016/j.atmosenv.2023.120199.

References

Amos, H.M., Jacob, D.J., Holmes, C.D., Fisher, J.A., Wang, Q., Yantosca, R.M., et al., 2012. Gas-particle partitioning of atmospheric Hg(II) and its effect on global mercury deposition. Atmos. Chem. Phys. 12, 591–603.

Beckers, F., Rinklebe, J., 2017. Cycling of mercury in the environment: sources, fate, and human health implications: a review. Crit. Rev. Environ. Sci. Technol. 47, 693–794.

Ding, A.J., Huang, X., Nie, W., Chi, X.G., Xu, Z., Zheng, L.F., et al., 2019. Significant reduction of PM2.5 in eastern China due to regional-scale emission control: evidence from SORPES in 2011-2018. Atmos. Chem. Phys. 19, 11791–11801.

Fu, X., Yang, X., Lang, X., Zhou, J., Zhang, H., Yu, B., et al., 2016. Atmospheric wet and litterfall mercury deposition at urban and rural sites in China. Atmos. Chem. Phys. 16, 11547–11562.

Fu, X.W., Zhang, H., Yu, B., Wang, X., Lin, C.J., Feng, X.B., 2015. Observations of atmospheric mercury in China: a critical review. Atmos. Chem. Phys. 15, 9455–9476.

Holmes, C.D., Jacob, D.J., Corbitt, E.S., Mao, J., Yang, X., Talbot, R., et al., 2010. Global atmospheric model for mercury including oxidation by bromine atoms. Atmos. Chem. Phys. 10, 12037–12057.

Horowitz, H.M., Jacob, D.J., Zhang, Y., Dibble, T.S., Slemr, F., Amos, H.M., et al., 2017. A new mechanism for atmospheric mercury redox chemistry: implications for the global mercury budget. Atmos. Chem. Phys. 17, 6353–6371.

Li, R., Wu, H., Ding, J., Fu, W., Gan, L., Li, Y., 2017. Mercury pollution in vegetables, grains and soils from areas surrounding coal-fired power plants. Sci. Rep. 7, 46545.

Liu, K., Wu, Q., Wang, L., Wang, S., Liu, T., Ding, D., et al., 2019. Measure-specific effectiveness of air pollution control on China's atmospheric mercury concentration and deposition during 2013-2017. Environ. Sci. Technol. 53, 8938–8946.

Liu, S., Wang, X., Guo, G., Yan, Z., 2021. Status and environmental management of soil mercury pollution in China: a review. J. Environ. Manag. 277.

Obrist, D., Kirk, J.L., Zhang, L., Sunderland, E.M., Jiskra, M., Selin, N.E., 2018. A review of global environmental mercury processes in response to human and natural perturbations: changes of emissions, climate, and land use. Ambio 47, 116–140.

Paatero, P., Tapper, U., 1994. Positive matrix factorization - a nonnegative factor model with optimal utilization of error-estimates of data values. Environmetrics 5, 111–126.

Pacyna, J.M., Travnikov, O., De Simone, F., Hedgecock, I.M., Sundseth, K., Pacyna, E.G., et al., 2016. Current and future levels of mercury atmospheric pollution on a global scale. Atmos. Chem. Phys. 16, 12495–12511.

Qin, X., Zhang, L., Wang, G., Wang, X., Fu, Q., Xu, J., et al., 2020. Assessing contributions of natural surface and anthropogenic emissions to atmospheric mercury in a fast-developing region of eastern China from 2015 to 2018. Atmos. Chem. Phys. 20, 10985–10996.

Saiz-Lopez, A., Sitkiewicz, S.P., Roca-Sanjuan, D., Oliva-Enrich, J.M., Davalos, J.Z., Notario, R., et al., 2018. Photoreduction of gaseous oxidized mercury changes global atmospheric mercury speciation, transport and deposition. Nat. Commun. 9, 4796.

Selin, N.E., Jacob, D.J., Yantosca, R.M., Strode, S., Jaegle, L., Sunderland, E.M., 2008. Global 3-D land-ocean-atmosphere model for mercury: present-day versus preindustrial cycles and anthropogenic enrichment factors for deposition (vol 22, artn no GB3099, 2008). Global Biogeochem. Cycles 22.

Shah, V., Jacob, D.J., Thackray, C.P., Wang, X., Sunderland, E.M., Dibble, T.S., et al., 2021. Improved mechanistic model of the atmospheric redox chemistry of mercury. Environ. Sci. Technol. 55, 14445–14456.

Song, Z., Wang, C., Ding, L., Chen, M., Hu, Y., Li, P., et al., 2021. Soil mercury pollution caused by typical anthropogenic sources in China: evidence from stable mercury isotope measurement and receptor model analysis. J. Clean. Prod. 288.

Streets, D.G., Horowitz, H.M., Lu, Z., Levin, L., Thackray, C.P., Sunderland, E.M., 2019. Global and regional trends in mercury emissions and concentrations, 2010–2015. Atmos. Environ. 201, 417–427.

Sun, P., Nie, W., Chi, X.G., Xie, Y.N., Huang, X., Xu, Z., et al., 2018. Two years of online measurement of fine particulate nitrate in the western Yangtze River Delta: influences of thermodynamics and N_2O_5 hydrolysis. Atmos. Chem. Phys. 18, 17177–17190.

Tang, Y, Wang, S, Wu, Q, Liu, K, Wang, L, Li, S, et al., 2018. Recent decrease trend of atmospheric mercury concentrations in East China: the influence of anthropogenic emissions. Atmos. Chem. Phys. 18, 8279–8291.

ten Brink, H, Otjes, R, Jongejan, P, Slanina, S, 2007. An instrument for semi-continuous monitoring of the size-distribution of nitrate, ammonium, sulphate and chloride in aerosol. Atmos. Environ. 41, 2768–2779.

Ulbrich, I.M., Canagaratna, M.R., Zhang, Q., Worsnop, D.R., Jimenez, J.L., 2009. Interpretation of organic components from Positive Matrix Factorization of aerosol mass spectrometric data. Atmos. Chem. Phys. 9, 2891–2918.

UN-Environment, 2019. Global Mercury Assessment 2018. UN Environment Programme. Chemicals and Health Branch, Geneva, Switzerlan.

UNEP, 2013. United Nations Environment Programme (UNEP): Minamata Convention on Mercury. UNEP: Minamata, Japan.

Wang, L., Chen, X., Zhang, Y., Li, M., Li, P., Jiang, L., et al., 2021. Switching to electric vehicles can lead to significant reductions of PM2.5 and NO2 across China. One Earth 4, 1037–1048.

Wang, X., Lin, C.-J., Feng, X., Yuan, W., Fu, X., Zhang, H., et al., 2018. Assessment of regional mercury deposition and emission outflow in Mainland China. J. Geophys. Res. Atmos. 123, 9868–9890.

Wang, X., Lin, C.-J., Yuan, W., Sommar, J., Zhu, W., Feng, X., 2016. Emission-dominated gas exchange of elemental mercury vapor over natural surfaces in China. Atmos. Chem. Phys. 16, 11125–11143.

Wu, P., Zakem, E.J., Dutkiewicz, S., Zhang, Y., 2020. Biomagnification of methylmercury in a marine plankton ecosystem. Environ. Sci. Technol. 54, 5446–5455.

Wu, Q., Li, G., Wang, S., Liu, K., Hao, J., 2018. Mitigation options of atmospheric Hg emissions in China. Environ. Sci. Technol. 52, 12368–12375.

Wu, Q.R., Wang, S.X., Li, G.L., Liang, S., Lin, C.J., Wang, Y.F., et al., 2016. Temporal trend and spatial distribution of speciated atmospheric mercury emissions in China during 1978-2014. Environ. Sci. Technol. 50, 13428–13435.

Wu, X., Fu, X., Zhang, H., Tang, K., Wang, X., Zhang, H., et al., 2023. Changes in atmospheric gaseous elemental mercury concentrations and isotopic compositions at Mt. Changbai during 2015-2021 and Mt. Ailao during 2017-2021 in China. J. Geophys. Res. Atmos. 128 (10) e2022JD037749.

Xu, X., Feng, X., Lin, H., Zhang, P., Huang, S., Song, Z., et al., 2022. Modeling the high-mercury wet deposition in the southeastern US with WRF-GC-Hg v1.0. Geosci. Model Dev. (GMD) 15, 3845–3859.

Zhang, L., Wang, S., Wang, L., Wu, Y., Duan, L., Wu, Q., et al., 2015a. Updated emission inventories for speciated atmospheric mercury from anthropogenic sources in China. Environ. Sci. Technol. 49, 3185–3194.

Zhang, Y., Jaeglé, L., van Donkelaar, A., Martin, R.V., Holmes, C.D., Amos, H.M., et al., 2012. Nested-grid simulation of mercury over North America. Atmos. Chem. Phys. 12, 6095–6111.

Zhang, Y., Song, Z., Huang, S., Zhang, P., Peng, Y., Wu, P., et al., 2021. Global health effects of future atmospheric mercury emissions. Nat. Commun. 12, 3035.

Zhang, Y., Zhang, L., Cao, S., Liu, X., Jin, J., Zhao, Y., 2023a. Improved anthropogenic mercury emission inventories for China from 1980 to 2020: toward more accurate effectiveness evaluation for the Minamata convention. Environ. Sci. Technol. 57, 8660–8670.

Zhang, Y., Zhang, P., Song, Z., Huang, S., Yuan, T., Wu, P., et al., 2023b. An updated global mercury budget from a coupled atmosphere-land-ocean model: 40% more re-emissions buffer the effect of primary emission reductions. One Earth 6, 316–325.

Zhang, Y.J., Tang, L.L., Wang, Z., Yu, H.X., Sun, Y.L., Liu, D., et al., 2015b. Insights into characteristics, sources, and evolution of submicron aerosols during harvest seasons in the Yangtze River delta region, China. Atmos. Chem. Phys. 15, 1331–1349.

Zhang, Y.X., Jacob, D.J., Horowitz, H.M., Chen, L., Amos, H.M., Krabbenhoft, D.P., et al., 2016. Observed decrease in atmospheric mercury explained by global decline in anthropogenic emissions. Proc. Natl. Acad. Sci. U.S.A. 113, 526–531.

Zhao, S., Pudasainee, D., Duan, Y., Gupta, R., Liu, M., Lu, J., 2019. A review on mercury in coal combustion process: content and occurrence forms in coal, transformation, sampling methods, emission and control technologies. Prog. Energy Combust. Sci. 73, 26–64.

Zheng, B., Tong, D., Li, M., Liu, F., Hong, C., Geng, G., et al., 2018. Trends in China's anthropogenic emissions since 2010 as the consequence of clean air actions. Atmos. Chem. Phys. 18, 14095–14111.

Zhu, W., Fu, X., Zhang, H., Liu, C., Skyllberg, U., Sommar, J., Yu, B., Feng, X., 2022. Mercury isotope fractionation during the exchange of Hg(0) between the atmosphere and land surfaces: implications for Hg(0) exchange processes and controls. Environ. Sci. Technol. 56 (2), 1445–1457.

Zhu, W., Li, Z., Li, P., Yu, B., Lin, C.J., Sommar, J., et al., 2018. Re-emission of legacy mercury from soil adjacent to closed point sources of Hg emission. Environ. Pollut. 242, 718–727.

Zhu, W., Lin, C.-J., Wang, X., Sommar, J., Fu, X., Feng, X., 2016. Global observations and modeling of atmosphere–surface exchange of elemental mercury: a critical review. Atmos. Chem. Phys. 16, 4451–4480.